

Classical ground states, spin-wave and PCUT analysis of H₂SQ system

Vikas Vijigiri^{1,2,*} and Saptarshi Mandal^{1,2,†}

¹*Institute of Physics, Bhubaneswar-751005, Orissa, India*

²*Homi Bhabha National Institute, Mumbai - 400 094, Maharashtra, India*

(Dated: September 1, 2018)

We study an organic Hydrogen bonded material H₂SQ analytically and map out the phase diagram as well as low energy excitations in the relevant parameter space. At zeroth order the dynamics is governed by plaquette interaction (product of σ_z over a plaquette) which defines a Z_2 gauge theory and a deconfinement phase satisfying "ice rules". The system is studied under additional interactions such as an external Zeeman field (with strength K) in x -direction, a inter-molecular interaction (with strength J_1) and a dipole-dipole interaction with strength J_2 such that $K > J_1 > J_2$. The effect of dipole-dipole interaction removes the local Z_2 symmetry and gives rise to four global degenerate states with Ferroelectric order. Using meanfield analysis we chart out the phase diagram for classical version of the model and find K_c which defines the transition from disordered phase to ordered phase in J_1, K plane for various values of J_2 . We find that presence of J_1 and J_2 tends to stabilize the deconfined phases. Over the classical ground states we perform spin-wave analysis and surprisingly find that quantum fluctuations does not remove the classical degeneracy at all at quadratic level. The spin-wave spectrum is found for the four global degenerate ground states which shows both gapped spectrum and gapless spectrum (near the vicinity of CDT transition) for $J_2 = 0$. However for J_2 finite, the spectrum is always gapped. We perform PCUT analysis to improve the results of spin-wave analysis and calculate ground state energy and one particle dispersion and gap at high symmetry point. Using this we draw the phase boundary between confined and deconfined phase in the $K - J_1$ plane. The effect of J_2 is also discussed in the resulting phase boundary.

PACS numbers: 75.10.Jm, 71.10.Pm, 03.65.Vf, 05.30.Pr

I. INTRODUCTION

The hydrogen-bonded systems continue to serve as a basis of realizing quantum effects at macroscopic scale¹⁻³, as these are the systems which exhibit quantum tunneling (of positively charged Hydrogen atoms) between two adjacent sites. The position of Hydrogen atoms are usually replaced by the pseudo-spin 1/2 variable which then can be mapped into suitable quantum spin systems, for example water spin ice system⁴. Among the various hydrogen bonded materials, the organic H₂SQ is notable for their ferroelectric properties, light weightness and eco friendly nature. The ferroelectric properties of such system was first studied by Slater on KH₂PO₄(KDP)¹. Later several experimental observations of the ferroelectric properties were observed in several hydrogen-bonded ferroelectrics^{2,3,5,6}. Recently there has been effort to provide a theoretical framework of these systems in the language of quantum spin systems⁷⁻⁹. To minimize free energy the position of Hydrogen atoms in these systems are inherently subjected to the constraint called "ice rules", which constraints exactly two hydrogen atoms are approaching oxygen atom out of four hydrogen atoms^{1,11-13}. Squaric acid molecule H₂SQ is a hydrogen bonded organic system which has a quasi two dimensional antiferroelectric layer where the square molecule SQ (say type A) is surrounded by four molecules of type B with hydrogen bonds⁶. This constraint is very much similar to the well known two-in and two-out configurations in Spin ice pyrochlores and other frustrated systems¹⁴. Such systems with the ice rule constraints are shown to exhibit

no long range ordering (LRO) down to zero temperature with exotic magnetic monopoles as the elementary excitations^{7,8,15-17}. The ice rules which are seen as the frustration in the system where all the configurations in the low energy sector are degenerate was discussed by Pauling in the early 1930s¹¹. While the quantum effects of the water ice and spin ice remains to attract us, the recent studies on water ice systems have shown to exhibit interesting phenomenon of coherent quantum tunneling in the low temperatures leading to U(1) Quantum Spin-liquid ground states with fractionalized spinon and gauge field excitations^{7,8,15-18}.

Here, in this paper we theoretically analyze the phase diagram and low lying excitations of H₂SQ systems in general at zero temperature. The earlier work⁶ investigated the finite temperature phase diagram in the $T - P$ plane where T is temperature and P is pressure. They have found a phase transition from AFE (anti-ferroelectric) to PE (paraelectric) phase. The paraelectric phase sustains at zero temperature above some critical pressure P_c . To our knowledge the first model Hamiltonian was proposed in Ref[13] which view the H₂SQ is an interacting one-dimensional Ising spin chains. Recently Chern et al⁹ has studied similar model Hamiltonian for such a system and obtained phase diagram numerically using quantum monte carlo technique at zero temperature. The Model Hamiltonian at zeroth order consists a four-spin plaquette interaction with a strength J_0 . This interaction give rise to so called "ice-rules" and defines a deconfined phase. When the Hamiltonian is studied in the presence of a magnetic field characterized by a param-

eter K , the system shows a confinement-deconfinement phase transition. The model also include a next-nearest neighbouring Ising like interaction with a strength J_1 and a dipole-dipole interaction $J_2 < J_1$. Usually the presence of J_2 causes the Ferroelectricity of the materials. The model was shown to exhibit both confinement-deconfinement (CDT) and ferroelectric quantum phase transition (FT) for appropriate set of parameters of the model Hamiltonian. However, in this work we carry out analytical calculations which has not been done so far. We have used three different complimentary techniques, mainly classical meanfield analysis, spin-wave approximations over classical ground states and PCUT (perturbative continuous unitary transformation¹⁹⁻²³) to improve the results obtained in spin-wave approximations to obtain a complete theoretical understanding of the model. Our plan of presentation is as follows. In section II, we introduce the model Hamiltonian and explain various terms present. Next, we analyze the classical version of the model Hamiltonian in section III following which the spin wave excitations are obtained next. The PCUT analysis has been presented in section V. The mapping of our model Hamiltonian to that of Kitaev's Toric code Hamiltonian²⁵ is discussed in section VI and we summarize our results at the end.

II. MODEL

We consider the following Hamiltonian given below⁹:

$$H = H_0 + H_1 + H_2 \quad (1)$$

where H_0, H_1 and H_2 are respectively given by

$$H_0 = J_0 \sum_p \sigma_1^z \sigma_2^z \sigma_3^z \sigma_4^z - K \sum_i \sigma_i^x \quad (2)$$

$$H_1 = J_1 \sum_p (\sigma_1^z \sigma_3^z + \sigma_2^z \sigma_4^z) \quad (3)$$

$$H_2 = -J_2 \sum_{\langle AB \rangle} \vec{P}_A \cdot \vec{P}_B \quad (4)$$

where σ_i^{α} 's are the Pauli matrices, P_A and P_B are the dipole moment vectors of molecule A and B respectively and the components of them are defined as follows,

$$P_{(A,B)x} = (\pm) \frac{1}{4} (\sigma_1^z + \sigma_2^z - \sigma_3^z - \sigma_4^z) \quad (5)$$

$$P_{(A,B)y} = (\pm) \frac{1}{4} (\sigma_2^z + \sigma_3^z - \sigma_1^z - \sigma_4^z) \quad (6)$$

where (+) is for molecule A and (-) is for molecule B. The summation of indices 'p' runs over all the plaquettes of the dual lattice (red) and i runs over all the spins in the dual lattice and $\langle AB \rangle$ indicates the nearest neighbor dipole-dipole interaction.

The parameter space of the Hamiltonian H is three dimensional with J_0 being the largest followed by K, J_1

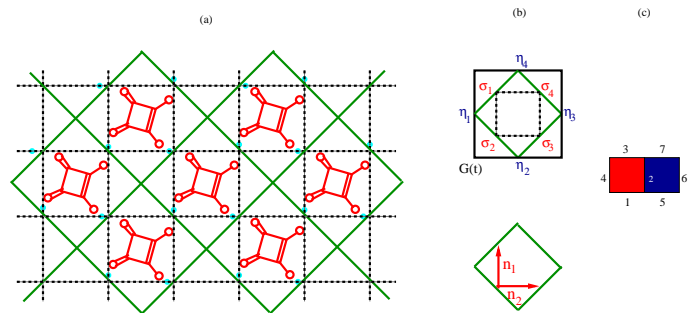


FIG. 1. The blue small dots represent the hydrogen atoms and the red circles represent the oxygen atoms of the molecule H_2SQ forming a quasi-2D configuration of hydrogen-bonded network. The top right corner showing the η variables defined on the dual lattice (green line) sites and the pseudo-spin variables σ which are defined on the bonds of the lattice (black dashed line).

and J_2 in magnitude. The ice rules were accounted in the form of \mathcal{Z}_2 gauge-invariant term $J_0 (> 0)$ and the intermolecular coupling term J_1 were generating a macroscopic degeneracy accounted in the form of Ising ferromagnet. Since there are ground states with each square plaquette having finite dipole moments, a more general Hamiltonian would also have these dipole-dipole interaction term J_2 .

III. CLASSICAL MODEL

In our endeavor to understand the different aspect of the complex Hamiltonian as given in Eqs. (1) - (4), we first examine the classical equivalent of the model where the quantum spins are now replaced by the classical Heisenberg spins. For sake of conveniences we rewrite the various terms in Eqs. 2-4 as follows,

$$H_0 = -\frac{1}{4} J_0 \sum_{\langle i_1 i_2 i_3 \rangle} S_{i_1}^z S_{i_2}^z S_{i_3}^z S_{i_4}^z - K \sum_i S_i^x \quad (7)$$

$$H_1 = \frac{1}{2} J_1 \sum_p (S_1^z S_3^z + S_2^z S_4^z) \quad (8)$$

$$H_2 = -\frac{1}{2} J_2 \sum_{\langle AB \rangle} \vec{P}_A \cdot \vec{P}_B \quad (9)$$

Following earlier study⁹, we assume that $J_0, J_1, J_2 > 0$ and the prefactors $\frac{1}{4}, \frac{1}{2}, \frac{1}{2}$ account for the multiple counting of the the same term in the Hamiltonian.

Let us briefly discuss the consequences of various terms in the above Hamiltonians. The first terms in H_0 can easily be satisfied by suitably aligning spins along $\pm z$ -axis such that each plaquette exactly contain two up-spins and two down spins which are equivalent to the celebrated ice-rules. If one considers a torus having \mathcal{N}_x and \mathcal{N}_y plaquette in x and y direction respectively then

there are $\mathcal{D} = 2^{N_x N_y}$ degenerate ground states for the first terms in the Hamiltonian. The 2nd largest scale problem i.e K brings in frustration in the tendency to align along the $\pm z$ -direction. As large K , all the spins are eventually aligned along the x -directions. One of our motivation to understand the classical version of the model was to investigate this transitions from highly degenerate classical configuration to a ordered phase where spins are along x -axis. The terms in H_1 and H_2 brings in additional complexity mainly by lifting the ground state degeneracy generated by first term in H partially. The term H_1 reduces the degeneracy \mathcal{D} to $\tilde{\mathcal{D}} = 2^{N_x N_y / 2}$ and dipole-dipole interaction eventually removes all local degeneracy causing a Ferroelectric alignment of electric dipoles associated with each plaquette. However there are four global degenerate states in this case which will be discussed later in detail.

Generally for classical Heisenberg type interactions, one resorts to Luttinger-Tisza method²⁶ to find the classical ground states. However the limitation of this approach is confined to only Bravais lattices, though for non-Bravais lattices, it may give important leads to possible ground state spin configurations²⁷. The presence of four-spin interactions limits us from using such analytical methods. Owing to this reason we examine numerically the ground state spin configurations. We notice that the Hamiltonian can be re-written in the following form²⁸ $H = \sum_i h_i^z S_i^z + h_i^x S_i^x$ where for a given spin-component S_i^α , h_i^α denotes the local field component along α -axis. The minimum energy configuration of spins are then obtained by aligning S_i^α to negative α -axis. Usually one starts from a random configurations of $[S_{i,0}^\alpha]$ yielding a configurations of $[h_{i,0}^\alpha]$ and a total energy $E[S_{i,0}^\alpha]$. The distribution $[h_{i,0}^\alpha]$ yields a new configurations of spins $[S_{i,1}^\alpha]$ and new total energy of the system $E[S_{i,1}^\alpha]$. In the above the index '0' and '1' denotes the steps in numerical iterations. We continue this process until $E[S_{i,n}^\alpha] \equiv E[S_{i,n+1}^\alpha]$. We have performed numerical simulations over lattice of dimension 256×256 and checked for sufficient initial configurations. Surprisingly we have found that the ground state has a one to one corresponds to the ground state configurations of the first terms of H_0 . The only difference is that the spins has now a finite and constant value of S_i^x which changes as a function of K and other parameters similar to what has been found for Kitaev model in the presence of transverse magnetic field in a earlier study²⁹. Thus the ground state configurations can be written as,

$$\vec{S}_i = S (\lambda_i \cos \theta \mathbf{e}_z + \sin \theta \mathbf{e}_x) \quad (10)$$

where λ_i could be \pm in tune with the ground state configurations of H_0 for $K = 0$. The value of θ depends on K, J_1, J_2 . For $K = 0$, we have $\theta = 0$. This θ takes the role of our order parameter. From the meanfield results represented by Eqn 10, the ground state energy of the

system can be written as follows,

$$E_{cl} = -\frac{1}{2} J_0 S^4 N \cos^4 \theta - J_1 S^2 N \cos^2 \theta - K S N \sin \theta - 2 J_2 S^2 N \cos^2 \theta \quad (11)$$

Minimizing E_{cl} with respect to θ we obtain θ_C which minimizes the ground state energy $E_{cl}(\theta_C)$. This ground state energy has been compared with the $E_x = -KN$ which denotes the energy corresponding to the state where all spins are aligned along x -direction. For a given J_0, J_1, J_2 there exists a K_c such that if $K \leq K_c$ then $E_{cl} < E_x(\theta_C)$ with $\theta_C \leq \frac{\pi}{2}$. Figure III shows the numerically obtained values of θ_C in $K - J_1$ plane for various values of J_2 . As evident from the Figure III, the value of K_c linearly increases with J_1 which is expected. As one increases the values of J_2 , K_C furthers takes higher value.

Let us summarize our results for classical ground state configurations. For all the parameter value there is a θ_C for $K \leq K_c$ which defines the ground state configurations according to the Eqn 10. The ground state has finite degeneracy in the presence of J_0, J_1 . For $J_1 = J_2 = 0$, the degeneracy is 2^N and for $J_2 = 0$, the degeneracy is $2^{N/2}$. For both J_1, J_2 nonzero, the degeneracy is reduced to 4 as described in Fig. IV B. For large $K > K_c$, all the spins get aligned along the x -axis corresponding to $\theta_C = \pi/2$. Now we are in a position to discuss the relative stability of the ground state spin configurations against the quantum fluctuation as prescribed by linear spin wave theory.

IV. LINEAR SPIN-WAVE THEORY

We notice that in general spins are quantized in an arbitrary direction which we call the local axis represented by x'/z' . The global axis will be represented by x/y . Any spins has the decomposition,

$$\vec{S}_{\mathbf{r}} = \tilde{\mathbf{e}}_x S_{\mathbf{r}}^x + \tilde{\mathbf{e}}_z S_{\mathbf{r}}^z \quad (12)$$

Here the index ' \mathbf{r} ' indicates the position of a given site. Now we perform an orthogonal co-ordinate transformation (from x, y, z to x', y', z') such that one axis of our new co-ordinate system gets aligned along the local moment direction at every site.

$$S_{\mathbf{r}}^x = S_{\mathbf{r}}^{x'} \cos \lambda_i \theta_c - S_{\mathbf{r}}^{z'} \sin \theta_c \quad (13)$$

$$S_{\mathbf{r}}^z = S_{\mathbf{r}}^{x'} \sin \lambda_i \theta_c + S_{\mathbf{r}}^{z'} \cos \theta_c \quad (14)$$

The expressions for $S_{x/z}^{\prime}$ in terms of the bosonic operators are given below,

$$S_{\mathbf{r}}^{x'} = s - a_{\mathbf{r}}^\dagger a_{\mathbf{r}}, \quad S_{\mathbf{r}}^{z'} = \sqrt{\frac{s}{2}} (a_{\mathbf{r}}^\dagger + a_{\mathbf{r}}) \quad (15)$$

We have specifically chosen the above representation as our interest is to investigate the phase boundary where

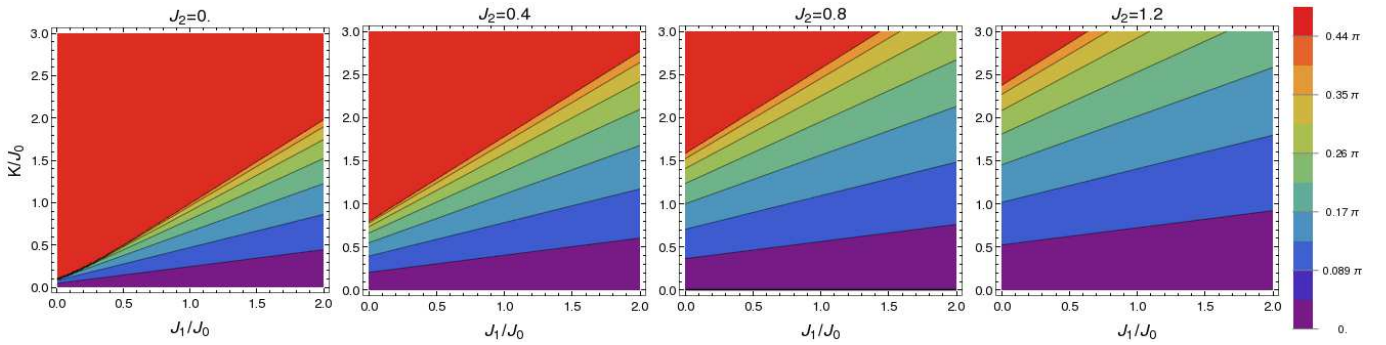


FIG. 2. In the above figure we have represented contour plot of θ_c in the $K - J_1$ plane for various values of J_2 . The red region denotes ordered phase where all the spins align in x -direction. Various other shaded region (except red) denotes a disordered phase where the z -component of spins are disordered.

the spins align mostly along x -direction. Where $a_{\mathbf{r}}^\dagger$ & $a_{\mathbf{r}}$ represents creation & annihilation operator for magnon at site \mathbf{r} .

A. High-field limit, $K \gg J_0, J_1, J_2, \theta_0 = \pi/2$

We use Holstein-Primakoff transformation given in Eqs. 13 where the quantum fluctuations are given in the form of hard-core bosons and performing the transformation individually around the degenerate classical ground states obtained in the previous section for different cases of $J_2 = 0$ and $J_2 \neq 0$ in the low-field limit we obtain the bosonic Hamiltonian given by,

$$H = N \sum_k \left[\xi_k \hat{a}_k \hat{a}_k^\dagger + \frac{\gamma_k}{2} (\hat{a}_k \hat{a}_{-k} + \hat{a}_k^\dagger \hat{a}_{-k}^\dagger) \right] + KSN \quad (16)$$

where,

$$\begin{aligned} \varepsilon_k &= \gamma_k + K - \frac{SJ_2}{8} \\ \gamma_k &= \frac{-S}{4} \left[J_2(2p_k^2 - 1) - 4(J_1 + J_2)p_k \right] \end{aligned} \quad (17)$$

where $p_k = \cos(k_x + k_y) \cos(k_x - k_y)$. Diagonalizing the Hamiltonian we obtain the magnon-spectra as given by,

$$E_k = \sqrt{\varepsilon_k^2 - \gamma_k^2}. \quad (18)$$

The spectrum is plotted for few parameters as shown in Fig IV A. To extract the low energy behaviour of the spectrum expand the spectrum around the minima i.e around X -points as $(k_x = -\frac{\pi}{2} + \delta_x, k_y = \frac{\pi}{2} + \delta_y)$. substituting this into Eq. 18 and Eq. 17 to obtain,

$$E_{\vec{\delta}} = \tilde{K}_1^{1/2} \sqrt{\tilde{K}_2 + 4(J_1 + 2J_2)|\vec{\delta}|^2} \quad (19)$$

where $\tilde{K}_1 = K - \frac{SJ_2}{8}$, $\tilde{K}_2 = (K - 2SJ_1 - \frac{29}{8}SJ_2)$. From the above expression it is clear that the spectrum remains

gapped with quadratic low energy dispersions for all parameters values except for the second order critical line given by $K_c = 2SJ_1 + \frac{29}{8}SJ_2$ for which the spectrum is gapless and linear around minima.

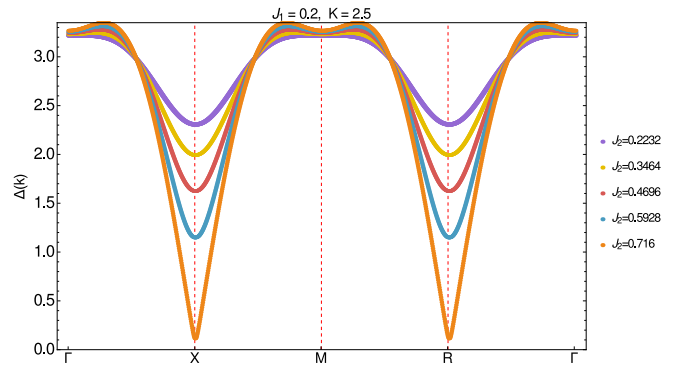


FIG. 3. Plot showing the dispersion in the High-field case, where quadratic behaviour slowly vanishes to a linear behavior at the second order critical line given by $K = 2SJ_1 + \frac{29}{8}SJ_2$.

B. Low-field case, $J_2 = 0, K$ is finite.

As mentioned before that when K is small compare to other parameters of the system and $J_2 = 0$, the classical ground state has huge degeneracy whose asymptotic dependence is $4\sqrt{N_p}$. To see their stability under quantum fluctuations, we performed the H-P transformation for each degenerate ground state and then numerically investigated whether the degeneracy is lifted and some states are selected as the ground states. We mention that these degenerate states has random dipole moment associated with each plaquette. To get the spectrum, we use wellknown dynamical matrix method ^{30,31} followed by equation of motion. The dynamical matrix is given

by,

$$i\frac{\partial\psi}{\partial t} = [\psi, H] = \mathcal{D}\psi \quad (20)$$

$$\psi^\dagger \equiv [a_1^\dagger \ a_2^\dagger \ \dots \ a_N^\dagger \ a_1 \ a_2 \ \dots \ a_N]$$

$$\begin{aligned} \mathcal{D}_{ii} &= 2J_0S^3 \cos^4 \theta + 2J_1S \cos^2 \theta + K \sin \theta \\ \mathcal{D}_{ij} &= -\lambda_i \lambda_j J_0 \frac{S^3}{2} \sin^2 \theta \cos^2 \theta + \delta \frac{SJ_1}{2} \sin^2 \theta \end{aligned} \quad (21)$$

where, λ_i 's are the coefficients obtained from the mean-field analysis and $\delta = 1$ if i, j belong to same plaquette and are along either one of the orthogonal directions n_1, n_2 else $\delta = 0$. Upon diagonalizing and picking the lowest eigenvalue we get the gap which is equal to 0.4581(4) for $J_0 = 1, J_1 = 0.2, K = 0.2$ and $\theta = 0.06691(5)$ which is in excellent agreement from the linear spin-wave calculations calculated for $J_2 \neq 0$ case whose ground states are subset of the degenerate ground states (DGS) for $J_2 = 0$ case as explained in Fig IV B. We have found that there is no lifting of degeneracy and the hence no order from disorder phenomenon happens here.

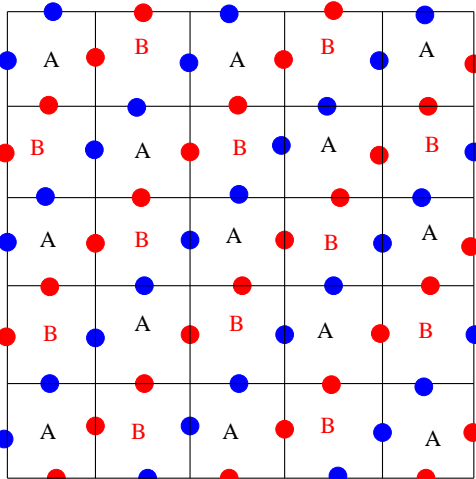


FIG. 4. One of the four degenerate ground states that exists for finite J_2 is shown in the above figure. The red dots represents up-spins and blue dots represents down-spins. Taking the mid points of the below left square as the origin, the position of up-spins and down spins can be written as $\vec{R}_{up} = -\tilde{e}_y/2 + m_1\vec{a} + n_1\vec{b}$, $\vec{R}_{down} = -\tilde{e}_x/2 + m_2\vec{a} + n_2\vec{b}$ where $\vec{a} = \tilde{e}_x/2 + \tilde{e}_y/2$, $\vec{b} = -\tilde{e}_x + \tilde{e}_y$. The 2nd degenerate ground state is obtained by replacing the up-spin by down-spins and vice versa. The third and fourth ground states could be obtained by rotating the spin-configuration of 1st and 2nd by $\pi/2$.

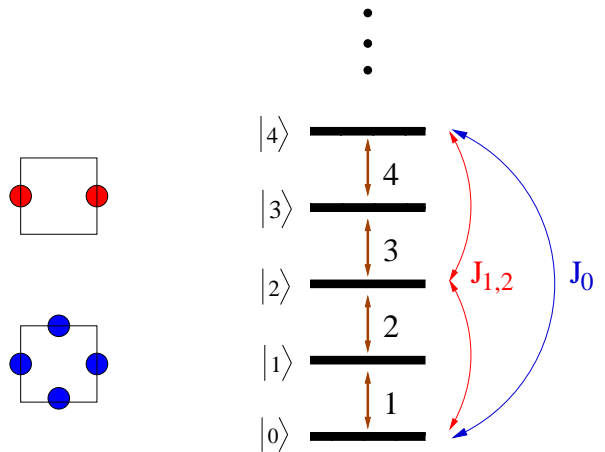


FIG. 5. Left column showing a cartoon picture of a process where the action of $T_2(4)$ (red(blue)) upon the ground state of 0-QP subspace producing 2-QP(above) and 4-QP(below) is shown. The right column shows a simple connection of the perturbing parameters connecting the different QP levels of the unperturbed Hamiltonian.

C. Low-field case, $J_2 \neq 0$

Similarly to previous sections here we perform a HP transformation around the ground states of ordered dimer coverings shown in Fig IV B.

$$\begin{aligned} H_i &= N \sum_k \left[\varepsilon_k a_k^\dagger a_k + \frac{\tilde{\gamma}_{i,k}}{2} (a_k^\dagger a_{-k}^\dagger + a_k a_{-k}) \right] \\ &\quad - \frac{1}{2} J_0 S^4 N C_\theta^4 - (J_1 + 2J_2) S^2 N C_\theta^2 \end{aligned} \quad (22)$$

where ε_k and $\gamma_{i,k}$ is given below,

$$\varepsilon_k = \gamma_k + 2S^3 J_0 C_\theta^4 + 2SJ_1 C_\theta^2 - \frac{J_2 S}{8} S_\theta^2 \quad (23)$$

$$\tilde{\gamma}_{i,k} = S_\theta^2 \left[\gamma_k + S^3 J_0 C_\theta^2 [2\chi_i q_k + p_k] \right] \quad (24)$$

In the above and $i = 1, 2, 3, 4$ corresponds to four degenerate ground states explained in Fig IV B. The value of $\chi_i = 1(-1)$ for $i = 1, 2(3, 4)$ and p_k, q_k, s_k are defined below. In the above C_θ and S_θ stands for $\cos \theta$ and $\sin \theta$ respectively and $q_k = \sin k_x \sin k_y$ and p_k is defined after Eq [17]. The spectrum is found gapped for all values of K, J_2 and given by

$$\Delta_k = \zeta_0 \sqrt{\zeta_1 + \zeta_2 \ell^2}$$

where $\zeta_0 = (2S^3 J_0 \cos^4 \theta + 2S(J_1 + 2J_2) \cos^2 \theta - \frac{SJ_2}{8} \sin^2 \theta)^{0.5}$, $\zeta_1 = 2J_1(S \cos^2 \theta - \frac{S}{2} \sin^2 \theta) + 8S^3 J_0 \cos^4 \theta - (2\chi + 1) \frac{S^3 J_0}{2} \cos^2 \theta \sin^2 \theta - \frac{15S}{8} J_2 \sin^2 \theta$ and $\zeta_2 = \frac{\sin^2 \theta}{2} \left[4S(J_1 + 3J_2) + 2S^3 \chi J_0 \cos^2 \theta \right]$. The constant of relevance here ζ_1 was solved numerically and

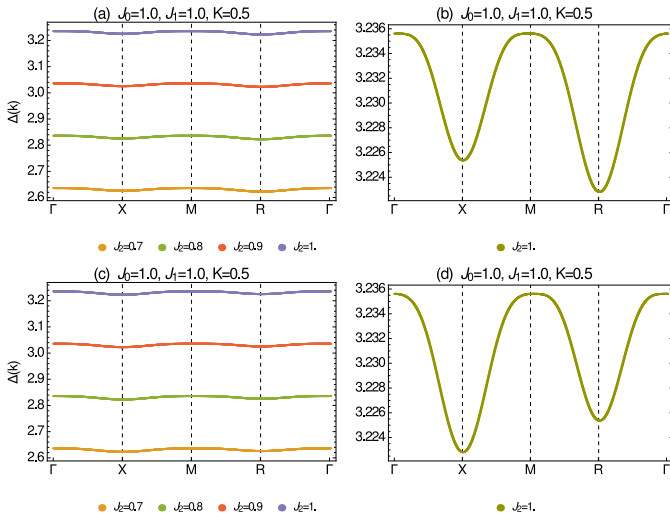


FIG. 6. In the above figure we have plotted the spin-wave dispersion for low values of K . The upper right panel (b) shows the spectrum for 1st and 2nd degenerate ground states as mentioned in Fig. IV B. Similarly lower right panel (c) shows the spectrum for 3rd and 4th ground states. The upper (a) and lower left columns (d) shows the variations of spectrum for different values of J_2 .

simultaneously with the equation that minimizes the total energy given in eqn.(11). The results for few parameter values are shown in Fig. ?? and we see the quadratic behavior for all the parameters values about the X,R-High symmetry points for ground states oriented along the $\pm x, \pm y$ respectively.

V. PCUT

The Hamiltonian as represented by Eq. 1 and equations following that represent in general a quantum interacting spin system which is often not solvable exactly. Generally one follows various analytical schemes depending on their interest of specific aspect of the model or the suitability of the model to the method itself. For example for one dimensional nearest neighbour interacting spin system Jordan-Wigner transformation³² is a very good starting point for analytical solutions. For 2 dimensional and in higher dimensional system in general slave fermion/boson methods are applied and often meanfield approximations are followed³³. Though there are exceptions for example Kitaev model^{24,25} which represents an exactly solvable model. As mentioned before, in this article we use PCUT (perturbative continuous unitary transformation) in our model whenever applicable. We are motivated by the fact that unlike slave boson/fermion formalism, we do not have to use meanfield approximations which is often does not represents the true ground states, on the otherhand few properties like gap and one particle spectrum can be calculated to very high order of perturbations as shown in previous studies³⁴. Another

important aspects of PCUT is the sequential derivations of effective Hamiltonian at higher order within a given particle sectors. The pre-requisite of applicability of PCUT is the equidistant spectrum which we have in the limit $K \gg J_0, J_1, J_2$ where the ground state is given by the spins aligned along the x -axis and excitations are given by spin flip excitations. We use PCUT to obtain the accurate measure of zero-particle gap and one particle dispersion and effective Hamiltonian upto reasonably high order. We compare our results of gap with previous monte-carlo studies⁹ and find very good comparison. Our one particle dispersion should also be useful to verify the low energy excitations beyond spin-wave approximations. Before we start the application of PCUT we first map the spin-Hamiltonian (1) onto the effective bosonic operator formalism. Since the ground state in the high-field limit is where all the spins are along x -axis, we transform our global z -basis along the ground state orientation of spin as:

$$S^x_{\mathbf{r}} = S^{x'}_{\mathbf{r}} \cos \theta - S^{z'}_{\mathbf{r}} \sin \theta \quad (25)$$

$$S^z_{\mathbf{r}} = S^{x'}_{\mathbf{r}} \sin \theta + S^{z'}_{\mathbf{r}} \cos \theta \quad (26)$$

where $\theta = \pi/2$, the expressions for $S'_{x/z}$ in terms of the bosonic operators are given below,

$$S^x_{\mathbf{r}} = s - a^\dagger_{\mathbf{r}} a_{\mathbf{r}}, \quad S^z_{\mathbf{r}} = \sqrt{\frac{s}{2}} (a^\dagger_{\mathbf{r}} + a_{\mathbf{r}}) \quad (27)$$

We now proceed to establish PCUT for our Hamiltonian (1) using Eqs 25. The resulting Hamiltonian has quadratic and as well quartic interaction which amounts to an interacting Hamiltonian. Our aim is to transform the resulting Hamiltonian to an unitarily equivalent Hamiltonian (H_{eff}) through a unitary transformation. Specifically, We follow the reference²³ where the block-band diagonality of the Hamiltonian is preserved with the choice of quasi-particle (QP) conserving infinitesimal generator $\eta(\ell)$ given by Wegner. We request the reader to follow the references for further pedagogical review. In the bosonic operator representation, the initial Hamiltonian (1) takes the form:

$$H = -\frac{N}{2} + Q + T_{-4} + T_{-2} + T_0 + T_2 + T_4 \quad (28)$$

where, $T_4 \propto J_0$, $T_2 \propto J_1, J_2$ are the effective operators corresponding to the perturbed Hamiltonian in the bosonic operator representation and Q is unperturbed Hamiltonian whose eigenstates serve as the basis for the Hilbert space of our system with $[Q, T_n] = nT_n$. Using eqns. (25), (27) the exact expressions for the effective operators T_n can be found as,

$$\begin{aligned}
T_0 &= J_0 \sum_{\square} [a_1 a_2 a_3^\dagger a_4^\dagger + a_1 a_2^\dagger a_3 a_4^\dagger + a_1 a_2^\dagger a_3^\dagger a_4 + \text{h.c.}] \\
&\quad + J_1 \sum_{\square} [a_1 a_3^\dagger + a_2 a_4^\dagger + \text{h.c.}] \\
&\quad + \frac{J_2}{8} \sum_{\langle AB \rangle} [a_2 a_4^\dagger + a_3 a_7^\dagger + a_1 a_5^\dagger + a_2 a_6^\dagger - a_3 a_7^\dagger \\
&\quad - a_1 a_7^\dagger - a_4 a_6^\dagger + \text{h.c.}] \\
T_2 &= J_0 \sum_{\square} [a_1^\dagger a_2 a_3^\dagger a_4^\dagger + a_1^\dagger a_2^\dagger a_3 a_4^\dagger + a_1^\dagger a_2^\dagger a_3^\dagger a_4 + a_1 a_2^\dagger a_3^\dagger a_4^\dagger] \\
&\quad + J_1 \sum_{\square} [a_1^\dagger a_3^\dagger + a_2^\dagger a_4^\dagger] \\
&\quad + \frac{J_2}{8} \sum_{\langle AB \rangle} [a_2^\dagger a_4^\dagger + a_3^\dagger a_7^\dagger + a_1^\dagger a_5^\dagger + a_2^\dagger a_6^\dagger - a_3^\dagger a_7^\dagger \\
&\quad - a_1^\dagger a_7^\dagger - a_4^\dagger a_6^\dagger] \\
T_4 &= J_0 \sum_{\square} [a_1^\dagger a_2^\dagger a_3^\dagger a_4^\dagger]
\end{aligned} \tag{29}$$

where the numbering is according to FIG. IIc. The conjugate operators can be found as $T_n^\dagger = T_{-n}$. With the effective operators in hand, the Hamiltonian (28) can now be transformed to an effective Hamiltonian $H_{\text{eff}} = U^\dagger H U$ commuting with Q . The infinitesimal unitary transformation is given by, $U \approx 1 + i\eta(\ell)$ where $\partial_\ell H = [\eta(\ell), H(\ell)]$ which determine the effective Hamiltonian in the limit $\ell \rightarrow \infty$. The above choice of generator is given in the pioneering work of Wegner^{22,23}. Starting from the Hamiltonian (28), we get the block-band diagonal effective Hamiltonian perturbatively order by order in our case. The general form of effective Hamiltonian can be represented as^{20,21}:

$$H_{\text{eff}} = -\frac{N}{2} + Q + \sum_{k=1}^{\infty} \sum_{\substack{|m|=k, \\ M(m)=0}} C(\underline{m}) T_{m_1} \cdots T_{m_k} \tag{30}$$

where the series expansion coefficients $c(\underline{m})$ are computed before hand using the flow equations. The next job in solving the Hamiltonian (30) is to determine it's action in each subspace of a given QP number q and diagonalize H_{eff} in each of these subspaces. In the following sections we computed the above Hamiltonian in the respective subspaces of $q = 0, 1$ and we present the results of ground state energy per spin ($q = 0$) and one particle gap ($q = 1$) in the confined phase ($J_2 = 0$) and paraelectric phase ($J_2 \neq 0$) respectively.

A. Large-field limit ($J_2 = 0, K \gg J_1, J_0$)

As mentioned in the outline, to determine the value of K_c we perform the PCUT method considering the low-energy sector of the Hamiltonian (1) in the strong-field

limit $K \gg J_0, J_1, J_2 = 0$ of CDT. The ground state (0-QP state) is fully polarized in the x-direction and the elementary excitations (1-QP state) are the single spin flips with energy cost $2K$, setting $K=1/2$ at order 7 we obtain the ground state energy and one-particle dispersion given by,

$$\begin{aligned}
e_0 &= -\frac{1}{2} - \frac{1}{8} J_0^2 - \frac{1}{384} J_0^4 - \frac{41}{393216} J_0^6 - \frac{1}{2} J_1^2 \\
&\quad - \frac{1}{2} J_0 J_1^2 - \frac{9}{32} J_0^2 J_1^2 - \frac{3}{16} J_0^3 J_1^2 - \frac{47525}{442368} J_0^4 J_1^2 \\
&\quad - \frac{1}{8} J_1^4 - \frac{1}{2} J_0 J_1^4 - \frac{32957}{32768} J_0^2 J_1^4 - \frac{61}{512} J_1^6
\end{aligned} \tag{31}$$

$$\begin{aligned}
\Delta &= 1 - \frac{1}{2} J_0^2 + \frac{3}{32} 3J_0^4 - \frac{1711}{27468} J_0^6 + 2J_0 J_1 + 2J_1 \\
&\quad - \frac{1}{8} J_0^2 J_1 - \frac{3}{4} J_0^3 J_1 + \frac{67}{576} J_0^4 J_1 + \frac{8131}{13824} J_0^5 J_1 \\
&\quad - \frac{3}{4} J_0^2 J_1^2 - \frac{7}{2} J_0^3 J_1^2 - \frac{111013}{36864} J_0^4 J_1^2 + J_0 J_1^3 \\
&\quad + \frac{317}{128} J_0^2 J_1^3 - \frac{13361}{4608} J_0^3 J_1^3 - \frac{10207}{3072} J_0^2 J_1^4 + \frac{79}{128} J_0 J_1^5
\end{aligned} \tag{32}$$

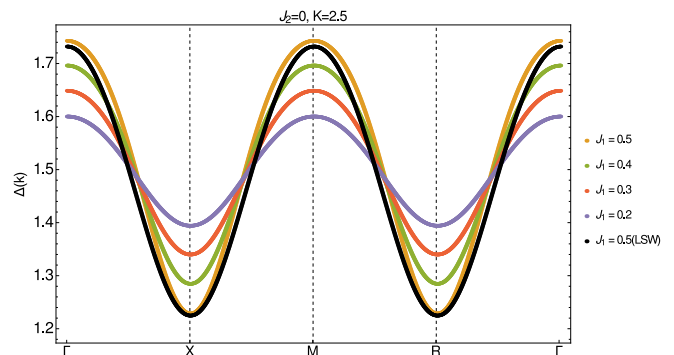


FIG. 7. Here we have plotted the spectrum as obtained from PCUT upto 7th order. The black line is the result obtained from spin-wave approximation.

A standard analysis for the gap Δ using DLogPade approximants suggests that below $J_0 = 0.8$ there were no closure of the gap. Suggesting the quantum phase transition below $J_0 = 0.8$ may not be of second order. However at $J_0 = 1.5$ we obtain the relation of critical line $K_c = 2.931(5)J_1$. In Fig. V A, we presented the phase diagram from confined to deconfined phase transition in $K - J_1$ plane. In Fig. V A, we have plotted the dispersion as obtained from PCUT and compared with spin wave spectrum obtained earlier which matches each other very well.

B. Large-field limit ($J_2 \neq 0, K \gg J_2, J_1, J_0$)

In this section, we present the results of ground state energy per spin and the one particle dispersion for $J_2 \neq$

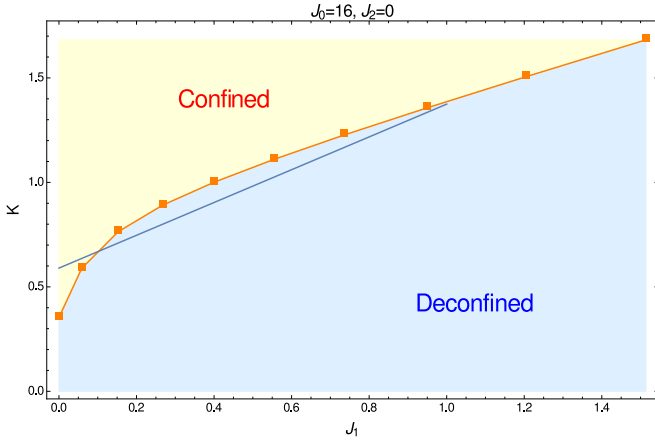


FIG. 8. The above figure shows the phase boundary between confined and deconfined phase as obtained by PCUT. The solid blue line is a linear regression fit of our PCUT result.

0. We could perform it till 4th order as the number of intermediate states increase due to non-local nature of dipole-dipole interaction. Nevertheless, the obtained expression are helpful in determining its critical behavior qualitatively. As in the above case the ground state is the state where all the spins are oriented along field-direction and the single-spin flips are the elementary excitations with $2K$ cost of energy, hence setting $K = 1/2$ we obtain the ground state energy and one-particle dispersion as,

$$\begin{aligned}
 e_0 = & -\frac{1}{8}J_0^2 - \frac{1}{384}J_0^4 - \frac{1}{2}J_1^2 - \frac{1}{2}J_0J_1^2 - \frac{9}{32}J_0^2J_1^2 - \frac{1}{8}J_1^4 \\
 & - \frac{1}{2}J_1J_2 - \frac{1}{2}J_0J_1J_2 - \frac{9}{32}J_0^2J_1J_2 - \frac{3}{8}J_1^2J_2 - \frac{3}{4}J_0J_1^2J_2 \\
 & - \frac{1}{4}J_1^3J_2 - \frac{3}{8}3J_2^2 - \frac{1}{8}J_0J_2^2 - \frac{39}{256}J_0^2J_2^2 - \frac{33}{32}J_1J_2^2 \\
 & - \frac{3}{2}J_0J_1J_2^2 - \frac{155}{64}J_1^2J_2^2 - \frac{15}{32}J_2^3 - \frac{9}{16}J_0J_2^3 \\
 & - \frac{207}{64}J_1J_2^3 - \frac{2859}{2048}J_2^4
 \end{aligned} \quad (33)$$

$$\begin{aligned}
 \Delta = & 1 + 2J_1 - \frac{1}{2}J_0^2 + \frac{3}{32}J_0^4 + 2J_0J_1 - \frac{1}{8}J_0^2J_1 - \frac{3}{4}J_0^3J_1 \\
 & - \frac{3}{4}J_0^2J_1^2 + J_0J_1^3 + J_0J_2 - \frac{3}{8}J_0^3J_2 + J_1J_2 + \frac{5}{2}J_0J_1J_2 \\
 & + \frac{105}{64}J_0^2J_1J_2 + \frac{3}{4}J_1^2J_2 + 3J_0J_1^2J_2 + \frac{1}{2}J_1^3J_2 \\
 & + \frac{11}{8}J_2^2 + \frac{41}{16}J_0J_2^2 - \frac{29}{128}J_0^2J_2^2 + \frac{45}{16}J_1J_2^2 \\
 & + \frac{233}{16}J_0J_1J_2^2 + \frac{71}{8}J_1^2J_2^2 + \frac{9}{4}J_2^3 + \frac{297}{32}J_0J_2^3 \\
 & + \frac{535}{32}J_1J_2^3 + \frac{553}{64}J_2^4
 \end{aligned} \quad (34)$$

Due to the increasing demand of computing power, we could only perform PCUT upto fourth order and find that gap does not vanishes unlike $J_2 = 0$ case. However this is fully consistent to that fact that switching on

J_2 triggers a para-electric phase as obtained in previous study⁹ which has excitations as a single dipole changing its direction costing a finite gap. Also in Fig. VB, we have plotted the dispersion as obtained from PCUT. We see that additional peaks appears in the dispersions when compared to spin-wave dispersions. This additional peaks denotes the emergence of paraelectric phase.

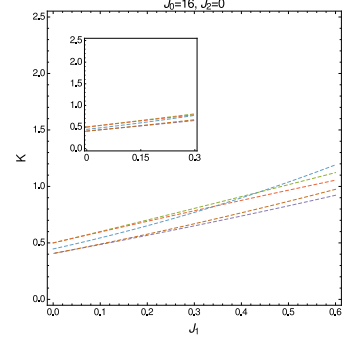


FIG. 9. The CDT transition in $K - J_1$ plane as obtained in various order of PCUT. The straight line which lie above are obtained in low order of PCUT. We see that at higher order it decreases the deconfined phase suggesting the success of PCUT to estimate the one particle gap closure effectively.

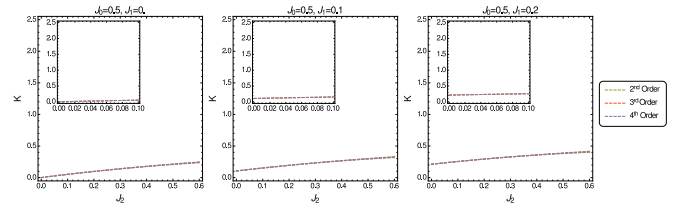


FIG. 10. The CDT as obtained for finite J_2 . We mention that the gap does not vanish really and the above plot is obtained from eq. 34 by solving for K_c from $\Delta = 0$.

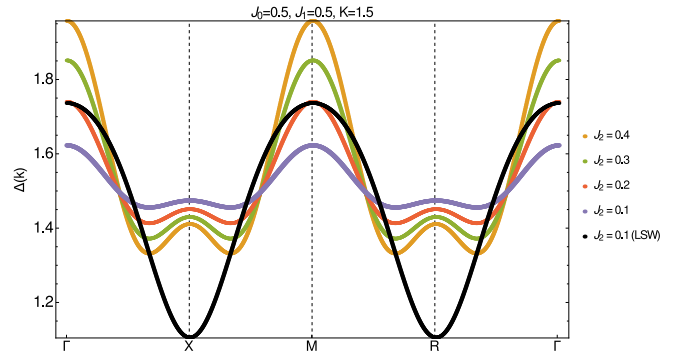


FIG. 11. In the above we have plotted one particle dispersion as obtained from PCUT. The above results is also compared with the spin-wave spectrum (the black plot). The additional peaks in the PCUT results suggests appearance of para-electric phase⁹ for the presence of finite J_2

Our results for gap and 1 particle dispersion will have

experimental consequences and can be verified. Below we discuss the model in the limit $J_0 \gg K$.

VI. DUAL MAPPING AND THE EXTENDED MODEL

As computed in a previous study³⁵ the model is shown to map to the celebrated Toric Code Model (TCM) in the low-field limit $J_0 \gg K_x$ and $J_{1,2} = 0$. Here for brevity we show the duality of the extended model where an extra field $K_y \ll J_0$ is applied along the transverse direction and show how it can be mapped to an interacting anyon model discussed in previous work³⁴.

$$H = -J_0 \sum_{\square} \sigma_1^z \sigma_2^z \sigma_3^z \sigma_4^z - K_x \sum_i \sigma_1^x - K_y \sum_i \sigma_1^y \quad (35)$$

In the limit $J_0 \gg K_{x,y}$ the Hamiltonian (35) can be transformed to an a transverse field model with a simple z-rotation. The new Hamiltonian in the transformed variables is given as,

$$H = -J_0 \sum_{\square} \sigma_1^{z'} \sigma_2^{z'} \sigma_3^{z'} \sigma_4^{z'} - K'_x \sum_i \sigma_1^{x'} \quad (36)$$

where $K'_x = (1 - \tan \theta)K_x$. Now for $J_0 > K'_x$ the Hamiltonian can be split as, $H = H_0 + H_1$ limit with the standard perturbation theory of using the projector operator formalism the effective Hamiltonian at 4th is

$$H_{\text{eff}}^{(4)} = \mathcal{P}(H_1 \mathcal{D})^3 H_1 \mathcal{P} \quad (37)$$

$$\mathcal{D} = -\frac{1 - \mathcal{P}}{H_0 - E_0}$$

using the eqns. (36),(37) the effective Hamiltonian can be found in our case as,

$$H_{\text{eff}}^{(4)} = -J_0 \sum_{\square} \sigma_1^z \sigma_2^z \sigma_3^z \sigma_4^z - \tilde{K} \sum_{+} \sigma_{\alpha}^x \sigma_{\beta}^x \sigma_{\gamma}^x \sigma_{\delta}^x \quad (38)$$

where $\tilde{K} = \frac{5K'_x}{16J_0^3}$ and the summation $+$ runs over all the vertices. The Hamiltonian (38) is nothing but the Toric Code Hamiltonian²⁵. In order to be in the deconfined ($K < 0.325J_0$) phase the coupling strengths should satisfy $\frac{5K'_x}{16J_0^3} < 0.325$. This mapping establishes a connection starting from Ising lattice gauge theory to Kitaev Hamiltonian²⁵. At fourth order, the anyons are non-interacting but beyonds 4-th order they becomes interacting as shown before³⁴. The implication of J_1 and

J_2 interaction on such interacting anyonic system is left as an future study.

VII. DISCUSSIONS

To summarize, in this study we have performed first ever analytical study of a model H_2SQ system. Our work builds on the model proposed earlier^{9,13}. To start with, we have clearly mentioned the various terms in the Hamiltonian and its physical origin. At the zeroth level, the model Hamiltonian has only plaquette term which harbors a deconfined phase. The application of an external magnetic field (given by a strength K) drives the deconfined phase to a confined phase. We have determined the value of K_c for which such transition happens. The role of intermolecular-coupling J_1 and dipole-dipole interaction J_2 on such transition has been investigated. We have shown that the role of J_1 and J_2 is to stabilize the deconfined phase. The ground state without dipole-dipole interaction term in the low field case was found to be singlet pair or dimers whose z-component projection of spin are anti-aligned to satisfy "ice-rules". Thus the classical ground state remains degenerate for small values of K . In the presence of the dipole-dipole term J_2 the local degeneracy has been removed to yield a four degenerate global ground states independent of system size. The role of quantum fluctuation has been investigated over these large classical degenerate ground states. Surprisingly we have found that, at quadratic level, the local degeneracy is not removed and there is no order from disorder phenomena occurs. We have found the spin-wave dispersion for the four global degenerate ground states and found that though in general the spectrum is gapped and quadratic for small values of k , for certain parameters, the spectrum becomes gapless and linear. This happens particularly near the phase boundary of confinement to deconfinement phase transition. Our formula for spin-wave dispersion and measure of gap will be useful for future experiment. To give a more meaningfulness to our study, we have applied PCUT to analysis the system in the large field limit ($K \gg J_0, J_1, J_2$) where the ground state consists of all spin aligned along x -direction and excitation consists of spin flip excitations. We have improved the estimation of ground state energy and one particle gap as estimated from spin-wave analysis. However we believe that further improvement of our work on PCUT can be done and it is left as a future study.

VIII. ACKNOWLEDGMENTS

We thank prof Julien Vidal for sharing his expertise on PCUT with us. We also thank Prof A. M. Jayannavar for encouraging us in the initial stages of this work.

* vikasvikki@iopb.res.in

† saptarshi@iopb.res.in

- ¹ J. C. Slater, *J. Chem. Phys.* **9**, 16 (1941).
- ² G. A. Samara, *Phys. Rev. Lett.* **27**, 103 (1971).
- ³ P. S. Peercy and G. A. Samara, *Phys. Rev. B* **8**, 2033 (1973).
- ⁴ Anderson, P. W., *Phys. Rev.* **102**, 1008 (1956).
- ⁵ G. A. Samara, *Ferroelectrics* **71**, 161 (1987).
- ⁶ Y. Moritomo, Y. Tokura, H. Takahashi, and N. Mori, *Phys. Rev. Lett.* **67**, 2041 (1991).
- ⁷ N. Shannon, O. Sikora, F. Pollmann, K. Penc, and P. Fulde, *Phys. Rev. Lett.* **108**, 067204 (2012).
- ⁸ N. Shannon, G. Misguich, and K. Penc, *Phys. Rev. B* **69**, 220403(R) (2004).
- ⁹ Chyh-Hong Chern and Naoto Nagaosa, *Phys. Rev. Lett.* **112**, 247602 (2014).
- ¹⁰ J. B. Kogut, *Rev. Mod. Phys.* **51**, 659 (1979).
- ¹¹ L. Pauling, *J. Am. Chem. Soc.* **57**, 2680 (1935).
- ¹² R. Savit, *Rev. Mod. Phys.* **52**, 453 (1980).
- ¹³ H.-D. Maier, H. E. Müser, and J. Petersson, *Z. Phys. B* **46**, 251 (1982).
- ¹⁴ C. Castelnovo, R. Moessner, and S. L. Sondhi, *Annu. Rev. Condens. Matter Phys.* **3**:35-55, (2012).
- ¹⁵ K. A. Ross, L. Savary, B. D. Gaulin and L. Balents, *Phys. Rev. X* **1**, 021002 (2011).
- ¹⁶ O. F. Syljuasen and S. Chakravarty, *Phys. Rev. Lett.* **96**, 147004 (2006).
- ¹⁷ E. Ardonne, P. Fendley, and E. Fradkin, *Ann. Phys. (Amsterdam)* **310**, 493 (2004).
- ¹⁸ C. Castelnovo, R. Moessner, and S. L. Sondhi, *Nature (London)* **451**, 42 (2008).
- ¹⁹ G. S. Uhrig and B. Normand, *Phys. Rev. B* **58**, R14705(1998).
- ²⁰ C. Knetter and G. S. Uhrig, *Euro. Phys. J. B* **13**, 209, (2000).
- ²¹ C. Knetter, K. P. Schmidt, and G. S. Uhrig, *Euro. Phys. J. B* **36**, 525 (2003).
- ²² F. Wegner, *J. Math. Phys.* **12**, 2259 (1971).
- ²³ F. Wegner, *Ann. Phys.* **3**, 77 (1994).
- ²⁴ A. Kitaev, *Annals of Physics*, **321**, 2–111 (2006).
- ²⁵ A. Kitaev, *Annals of Physics*, **303**, 2-30, (2003).
- ²⁶ J. M. Luttinger and L. Tisza, *Phys. Rev.* **70**, 954 (1946).
- ²⁷ S. Mandal, A. Andreanov, Y. Crespo, and N. Seriani, *Phys. Rev. B* **90**, 104420 (2013).
- ²⁸ S. R. Sklan and C. L. Henley, *Phys. Rev. B* **88**, 024407 (2013).
- ²⁹ Julien Vidal, Kai Phillip Schmidt, and Sébastien Dusuel, *Phys. Rev. B* **78**, 245121, (2008).
- ³⁰ J.H.P. Colpa, *Physica 93A* (1978) 327-353.
- ³¹ Ming-wen Xiao, arXiv:0908.0787.
- ³² Edurado Fradkin, *Phys. Rev. Lett* **63**, 322–325 (1989).
- ³³ X G Wen, *Phys. Rev. B* **65**, 165113, (2002).
- ³⁴ Julien Vidal, Ronny Thomale, Kai Phillip Schmidt, and Sébastien Dusuel, *Phys. Rev. B* **80**, 081104(R), (2009).
- ³⁵ Bo-Jie Huang and Chyh-Hong Chern, *IJMP B*, Vol. 31, No. 20 (2017) 1750130
- ³⁶ G. F. Reiter, J. Mayers, and P. Platzman, *Phys. Rev. Lett.* **89**, 135505 (2002).
- ³⁷ Y. Okimoto, R. Kumai, S. Horiuchi, H. Okamoto, and Y. Tokura, *J. Phys. Soc. Jpn.* **74**, 2165 (2005).
- ³⁸ H. W. J. Blote and Y. Deng, *Phys. Rev. E* **66**, 066110 (2002).
- ³⁹ K. G. Wilson, *Phys. Rev. D* **10**, 2445 (1974).
- ⁴⁰ Julien Vidal, Sebastien Dusuel and Kai Philip Schmidt, *Phys. Rev. B* **79**, 033109, (2009).